Active and Reactive Power Control Capability in Wind Generation based on BDFIG machine.

Pablo E. Troncoso[1] , Pedro E. Battaiotto and Ricardo J. Mantz[2]
Instituto LEICI
Facultad de Ingeniería, Universidad Nacional de La Plata
Buenos Aires, Argentina
troncosopablo08@yahoo.com.ar, pedro@ing.unlp.edu.ar, mantz@ing.unlp.edu.ar

***Abstract*— The paper deals with energy generation from wind turbines with brushless doubly-fed induction generators (BDFIG). The capability for reactive power generation, while the wind turbine captures maximum wind power, is particularly analyzed. The control-side converters regulate both active and reactive powers independently. The active power is described in terms to the mechanical power. The relation between reactive powers of the control and power windings is analyzed from curves obtained via simulations.**

***Index Terms*—BDFIG, Reactive Power Control, Maximum Power Point Tracking, Variable speed wind energy generation.**

I. INTRODUCTION

The Brushless Doubly Fed Induction Generator (BDFIG) arises as an alternative to the Permanent Magnet and Wound Rotor machines in wind energy conversion systems. Various works have addressed the study of this generator [1] - [5]. BDFIG consists in the two cascade induction machines with a common rotor. This configuration presents two three-phase windings with different numbers of pole pairs (called power and control windings) in the machine stator [7]. Because of the absence of slip rings and the possibility of reducing or even eliminating the gearbox, its utilization in wind turbine applications increases the system reliability and reduces the maintenance and the operational costs, which are of great importance in that kind of systems [3], [7]. Additionally, the power flow in the principal stator of the BDFIG could be driven from a fractional power converter connected on the auxiliary stator winding [8]-[9]. This makes the BDFIG especially attractive for wind energy systems working at variable speed. The control of BDFIG has some similarities with the control of DFIG, so allowing use some techniques and developing [8]. However, BDFIG also has structural differences that require the application the modern control concepts. Understanding of power capability of the BDFIG working how generator in variable speed drive wind generation applications is useful to determine control objectives. Generally, a strategy is required to control the active and reactive power injected or consumed from the mains to which it is connected [9], [11]. The strategies can modify set points in the controllers to meet demand of the grid.

This work analyzes the reactive power control capability of this machine in wind generation applications where maximum power is captured. The structure is as follows. Section 2 introduces the mathematical model of the BDFIG generator. Section 3 discusses the maximum power tracking problem in wind generation. Section 4 presents the control capability of this machine in wind energy generation, analyzing the power flow and the coupling between the electrical variables, and the section 5 presents simulation results. Finally, the conclusions are addressed.

II. MATHEMATICAL MODEL

The mathematical model of the electrical system relates the control and power windings variables of the DBFIG machine. It is represented by six dynamic voltage equations and the flux linkage equations. On the other hand the mechanical model is represented by the dynamical relation between the rotational speed, the electromagnetic torque and the input torque.

A. Electrical model

The power winding of the BDFIG generator is directly connect to the grid. In this context, the flux in the power winding remains approximately constant. Then, choosing the reference frame orientation coincident with the flux of the power winding [6], the *dq* voltage equations are

$$v_{qp} = r_p i_{qp} + \frac{d\lambda_{qp}}{dt} + \omega_e \lambda_{dp} \tag{1}$$

$$v_{dp} = r_p i_{dp} + \frac{d\lambda_{dp}}{dt} + \omega_e \lambda_{qp} \tag{2}$$

$$v_{qc} = r_c i_{qc} + \frac{d\lambda_{qc}}{dt} + [\omega_e - (p_p + p_c)\omega_r]\lambda_{dc} \tag{3}$$

$$v_{dc} = r_c i_{dc} + \frac{d\lambda_{dc}}{dt} + [\omega_e - (p_p + p_c)\omega_r]\lambda_{qc} \tag{4}$$

$$0 = r_r i_{qr} + \frac{d\lambda_{qr}}{dt} + (\omega_e - p_p \omega_r)\lambda_{dr} \tag{5}$$

[1]Consejo Nacional de Investigaciones Científicas y Técnicas (CONICET).
[2]Comisión de Investigaciones Científicas (CICpBA).

$$0 = r_r i_{dr} + \frac{d\lambda_{dr}}{dt} + (\omega_e - p_p \omega_r)\lambda_{qr} \quad (6)$$

and the flux linkage equations are

$$\lambda_{qp} = L_p i_{qp} + L_{mp} i_{qr} \quad (7)$$

$$\lambda_{dp} = L_p i_{dp} + L_{mp} i_{dr} \quad (8)$$

$$\lambda_{qc} = L_c i_{qc} - L_{mc} i_{qr} \quad (9)$$

$$\lambda_{dc} = L_c i_{dc} - L_{mc} i_{dr} \quad (10)$$

$$\lambda_{qr} = L_r i_{qr} + L_{mp} i_{qp} - L_{mc} i_{qc} \quad (11)$$

$$\lambda_{dr} = L_r i_{dr} + L_{mp} i_{dp} - L_{mc} i_{dc} \quad (12)$$

where the subscripts p, c and r stand for 'power winding', 'control winding' and 'rotor winding' quantities, respectively, and r_i, L_i and L_{mi} are the resistances, self-inductances and mutual inductances of the windings. The number of poles pairs is represented by p_i. Finally, ω_e and ω_r are the synchronous and rotational speed respectively.

B. Mechanical Model

The rotor of the machine rotates at a speed ω_r, being the mechanical dynamic equation

$$\frac{d\omega_r}{dt} = \frac{T_{in} - T_{em}}{J}, \quad (13)$$

where T_{in} is the input aerodynamic torque, J is the inertia of the system and T_{em} is the electromagnetic torque

$$T_{em} = \frac{3}{2} p_p L_{mp} (i_{qp} i_{dr} - i_{dq} i_{qr}) + \frac{3}{2} p_c L_{mc} (i_{qc} i_{dr} - i_{dc} i_{qr}). \quad (14)$$

The Fig.1 shows the steady state curve for BDFIG generator considered in this paper with the control winding shorted (i.e. v_c=0). The positive torque represents the machine working as generator and negative torque represents the machine working as motor.

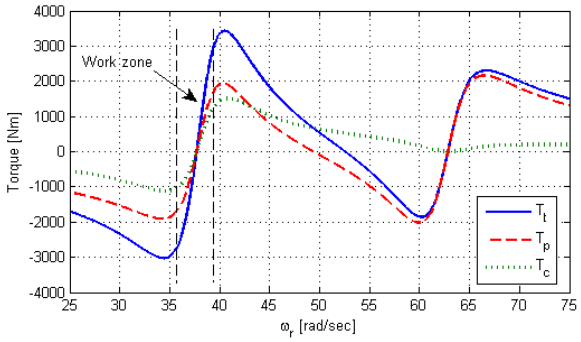

Figure 1. Total torque (solid line), torque of the power winding (dash line) and torque of the control winding (dotted line).

III. Maximum Power Tracking

The wind power capture is usually expressed in terms of the turbine power coefficient. In this context, assuming a constant wind speed v and an air density ρ, a wind turbine of blade length r capture a wind power

$$P(\lambda) = \frac{1}{2}\pi\rho r^2 C_p(\lambda) v^3, \quad (15)$$

where the power coefficient $C_p(\lambda)$ is a non-linear function of the tip speed ratio λ. This non-linear function presents a unique maximum in $\lambda = \lambda_{opt}$. Therefore, to achieve maximum wind power extraction, the rotational speed of the turbine should be controlled according wind speed variations.

In order to avoid measuring the wind speed, wind power is usually approached in terms of the aerodynamic torque [7], [11]. From (15) the aerodynamic torque

$$T(\lambda) = \frac{1}{2}\pi\rho r^2 \frac{C_p(\lambda)}{\lambda} v^2. \quad (16)$$

Replacing $\lambda = \lambda_{opt}$ and $v = r\omega_r / \lambda_{opt}$, the torque reference can be express as

$$T(\omega_r) = \frac{1}{2}\pi\rho r^5 \frac{C_p(\lambda_{opt})}{\lambda_{opt}^3} \omega_r^2, \quad (17)$$

The variation of the aerodynamic torque vs rotational speed and the optimal torque curve are presents in Fig. 2. The generator characteristics for different control voltages v_c are also depicted. The steady state curves of the generator are useful for understanding the system behavior and for its sizing. Among others, a difference between BDFIG and the classical DFIG lies in the possible steady state points where the system can work.

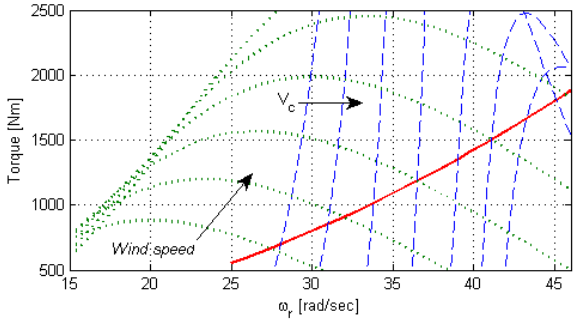

Figure 2. Wind torque variation for different wind speeds (dotted line), geometric place of the optimal torque (solid line) and generator steady state curves (dash line).

IV. CONTROL CAPABILITY

The BDFIG-WECS in the slip power recovery topology is described in the Fig. 3. The power winding is connected directly to the grid and the control winding is connected to the grid via a bidirectional converter in *back to back* configuration.

The control of the active and reactive powers is realized through the control-side converter, which imposes the currents of the control winding. [6], [7].

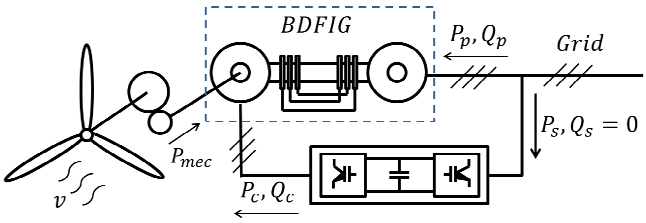

Figure 3. Power flow in the BDFIG-WECS with the slip power recovery.

A. Analysis of the Active and Reactive Power Expressions

In this work, an oriented vector method is adopted, where the *d*-axis of power winding reference is aligned with power winding flux. The axis d_p is aligned with the power windings flux λ_p, such that $\lambda_p = \lambda_{dp}$ and $\lambda_{qp} = 0$.

Using (1) - (12) and the frame chosen, the dynamic relations between the currents of the control winding and power winding currents are

$$\frac{di_{qc}}{dt} = -\frac{L_p r_r}{L_{mp} L_{mc}} i_{qp} - \frac{\sigma L_r L_p}{L_{mp} L_{mc}} \frac{di_{qp}}{dt} - \omega_1 i_{dc} - \frac{\sigma L_r L_p}{L_{mp} L_{mc}} \omega_1 i_{dp} + \frac{L_r}{L_{mp} L_{mc}} \omega_1 \lambda_p \quad (18)$$

$$\frac{di_{dc}}{dt} = -\frac{L_p r_r}{L_{mp} L_{mc}} i_{dp} - \frac{\sigma L_r L_p}{L_{mp} L_{mc}} \frac{di_{dp}}{dt} - \omega_1 i_{qc} - \frac{\sigma L_r L_p}{L_{mp} L_{mc}} \omega_1 i_{qp} + \frac{L_r}{L_{mp} L_{mc}} \frac{d\lambda_p}{dt} \quad (19)$$

where

$$\omega_1 = \omega_e - p_p \omega_r \quad (20)$$

$$\sigma = 1 - \frac{L_{mp}^2}{L_p L_r} \quad . \quad (21)$$

The expressions of active and reactive power equations in *dq* frame are

$$P_p = \frac{3}{2}(v_{qp} i_{qp} + v_{dp} i_{dp}) \quad (22)$$

$$Q_p = \frac{3}{2}(v_{qp} i_{dp} - v_{dp} i_{qp}) . \quad (23)$$

Using (1)-(12), (18)-(21) and the steady state equations and substituting into (22) and (23), the active and reactive powers in the power winding are obtained, which are affected by the currents components i_{qc} and i_{dc} as

$$P_p = \frac{3}{2}\frac{\omega_e}{\sigma L_r L_p}(-\frac{r_r}{\omega_1}\lambda_p^2 - L_{mp} L_{mc} \lambda_p i_{qc}) \quad (24)$$

$$Q_p = \frac{3}{2}\frac{\omega_e \lambda_p}{\sigma}(\frac{1}{L_p}\lambda_p - \frac{L_{mp} L_{mc}}{L_r L_p} i_{dc}) \quad (25)$$

Similarly, the equation (14) can be expressed in terms of the direct and quadrature currents of the control winding as

$$T_{em} = \frac{3}{2} i_{qp}(p_c \frac{L_{mc} L_p}{L_{mp}} i_{dc} + p_p \lambda_p) + \frac{3}{2} \frac{p_c L_{mc}}{L_{mp}} i_{qc} . \quad (26)$$

Equations (24)-(26) show the triangular coupling between the reactive power and the electromagnetic torque.

B. Analysis of the Active and Reactive Power Flows

The steady state active and reactive powers can be controlled independently by the direct and quadrature currents of the control winding.

In Fig. 3 shown as the power is distributed in the BDFIG, which can be seen as two DFIG machines connected in cascade. If the losses are not considered, the active power balance can be described as

$$P_p + P_c + P_{mec} = 0 \ . \quad (27)$$

This simplification allows interpreting easily the BDFIG behavior and the simulations results.

In the case of reactive power, it is useful to interpret the machine as a quadripole like a Fig. 4.

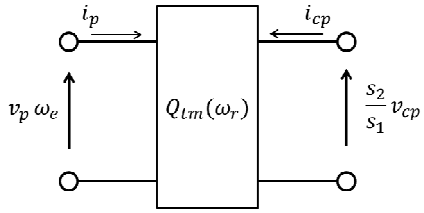

Figure 4. BDFIG represented as quadripole.

where s_1 and s_2 are the slips in the power and control windings respectively, v_p and v_{cp} are the power winding voltage and control winding voltage referred to the power winding and i_p and i_{cp} are the currents referred to power winding.

Then, the relation between reactive powers in the control and power windings is

$$Q_c = Q_{tm}(\omega_r) - Q_p \frac{s_1}{s_2}. \quad (28)$$

and taking in mind the BDFIG relation between slips are described to

$$\frac{s_1}{s_2} = 1 - \frac{\omega_r}{\omega_n}, \quad (29)$$

results

$$Q_c = Q_{tm}(\omega_r) + Q_p\left(\frac{\omega_r}{\omega_n} - 1\right). \quad (30)$$

The equation (30) represented the capability to generate Q_p VArs in the power winding with Q_c VArs in control winding for ensuring the $Q_{tm}(\omega_r)$ VArs necessary for magnetization the machine by the control winding.

The reactive power depends on the control winding voltage and the difference between the rotational speed and the synchronous speed. When this difference increases, more voltage is required in the control winding to generate VArs in power winding. This fact allows establish criteria for sizing the converters [10].

V. RESULTS

Curves that characterizes the control of the generator along the optimal torque curve with the simultaneous control of reactive power in the power winding is presented. The curves are obtained from controlling the generator with a robust technic based on *Higher Order Sliding Modes* algorithm (see Appendix). The wind turbine was sizing to obtain the maximum mechanic power P_{mec}=*100 KW* at $\omega_r = 47\, rad/\sec$. The power winding is connected to the 440 V_{rms} line voltage and 60 *Hz* grid, the control winding is connected to the grid via a PWM converter.

The control objectives are fulfilled when the control-side converter modifies the control current to satisfy the torque and reactive power requirement. Three requirements for reactive power in the power windings were established: $Q_p = 0$, $Q_p = 24KVAr$ and $Q_p = -24KVAr$. The torque reference is the optimal torque available in the wind. The gearbox relation is K_{gb}=4, the blades length is *r=8* m and the wind speeds varies between *5 m/sec* and *12 m/sec*.

The Fig. 5 shows the active power in the control and power windings. The sum of P_p and P_c is approximated to the available P_{mec} across the optimal torque curve. The Fig. 6 shows the reactive power Q_c in the power winding for different reference in Q_p. The VArs to operate the generator are injected from the control winding to minimization the reactive power consumed to the grid.

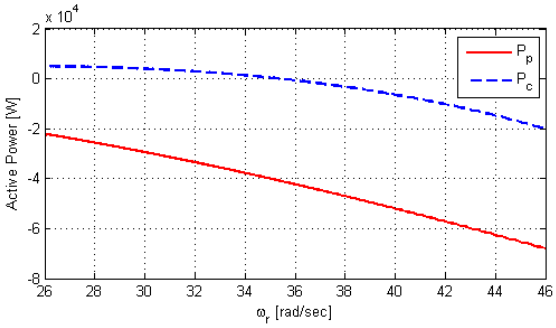

Figure 5. Active power in the power and control windings.

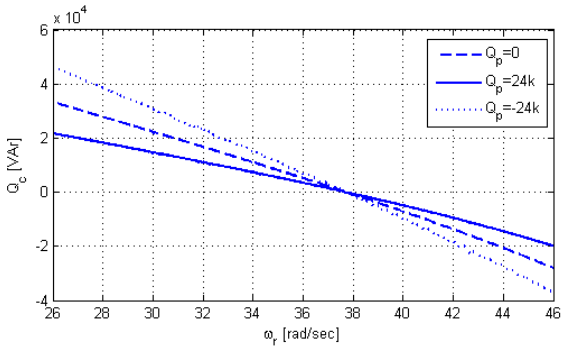

Figure 6. Reactive power in the power winding.

The Fig. 7 and Fig. 8 depicts the current in the windings and the RMS voltage to the control signal to $Q_p = 0$. In Fig.7 can be seen the RMS currents in the windings. The RMS current in the control winding is constant in the work range. The RMS current in the control winding follows a parabolic profile.

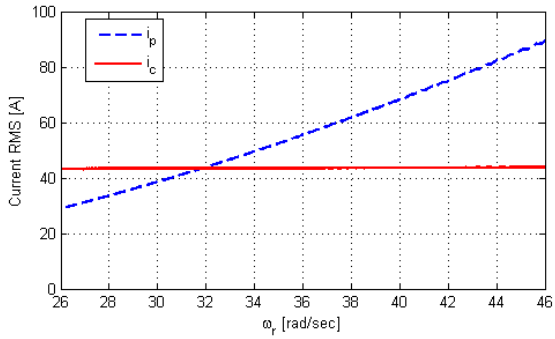

Figure 7. RMS current in the control and power windings.

These profiles in the windings due to the control action (i.e. the voltage applied to the control winding) are represented in the Fig. 8.

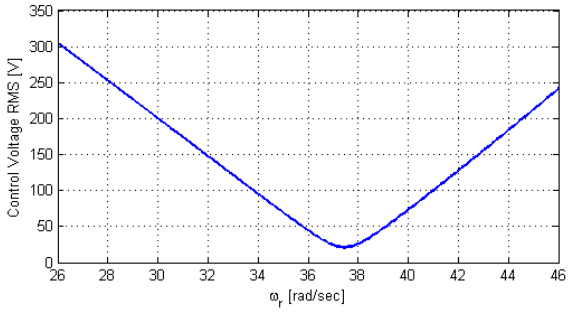

Figure 8. RMS voltage to the control signal per phase.

Note that is necessary to change the sign of the slope of the control voltage in order to control reactive power while wind power capture is maximized in all range of wind speeds. In concordance with Fig. 5 to Fig. 8, the Fig. 9 shows the apparent power in the control and power windings.

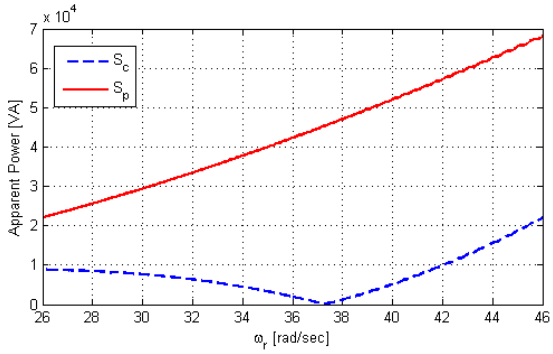

Figure 9. Apparent power in the stator windings.

CONCLUTIONS

The BDFIG expressions for active and reactive powers in function of the control winding currents show that is possible to propose and separate targets for active and reactive powers in steady state. The BDFIG machine displays a triangular coupling between the reactive power and electromagnetic torque indicating the convenience of using robust control techniques to improve system performance.

Due to the amplification effect between the control and power windings, it is concluded that it is appropriate to magnetize the machine from the control winding. Thus, the power winding can be used to wind power exchange and possibly exchanging reactive power with the network. BDFIG machine maintains a power ratio P_c / P_p similar to that of a DFIG, therefore common criteria for the design of converters can be used. Potentially, the study allows to propose control strategies for the entire working range of the machine, taking advantage of knowledge of extensively studied topologies. Understanding of reactive power capability of the BDFIG in wind generation applications is also useful for incorporating control objectives for reducing losses in the winding resistances and as a consequence to improve the system performance.

APPENDIX

A. *Control Techniques for the Torque and Reactive Power Capability Caracterization.*

The controller is designed to use a technique based on a *high order sliding mode* (particularly, "second order sliding mode" or SOSM) for MIMO systems.

Using (24) and (25) can find two sliding manifold to satisfy the control objectives. In this context the sliding surfaces can be expressed as

$$s_1 = T(\omega_r) - \frac{3}{2} i_{qp} \left(p_c \frac{L_{mc} L_p}{L_{mp}} i_{dc} + p_p \lambda_p \right) + \frac{3}{2} \frac{p_c L_{mc}}{L_{mp}} i_{qc} \tag{31}$$

$$s_2 = Q_{ref} - \frac{3}{2} \frac{\omega_e \lambda_p}{\sigma} \left(\frac{1}{L_p} \lambda_p - \frac{L_{mp} L_{mc}}{L_r L_p} i_{dc} \right) \tag{32}$$

where $T(\omega_r)$ is the optimal torque expressed by (17) and Q_{ref} is a reference for reactive power to satisfy the grid requirement.

The control signal is

$$u_i = w_i + \gamma_i \, | \, s_{0i} \, | \, sign(s_i) \tag{33}$$

$$w_i = \begin{cases} -\lambda_i \, | \, s_{0i} \, |^{\alpha} \; sign(s_i) & \text{si} \quad |s_i| > s_{0i} \\ -\lambda_i \, | \, s_i \, |^{\alpha} \; sign(s_i) & \text{si} \quad |s_i| \leq s_{0i} \end{cases} \tag{34}$$

where λ_i, γ_i and s_{0i} are design parameters that satisfies the next equations

$$\begin{matrix} \gamma_i > C_i / \Gamma_{mi} \\ \lambda_i > \sqrt{2(\gamma_i \Gamma_{Mi} + C_i)} / \Gamma_{mi} \end{matrix} , \quad \ddot{s}_i \in [-C_i, C_i] + [\Gamma_{mi}, \Gamma_{Mi}] \dot{u}_i \tag{35}$$

If (35) is satisfied for all sliding surfaces, the SOSM exist and the control objectives are satisfied. In [11] shows a demonstration to how tuning the gains of the "Super Twisting Controller" in coupled systems.

ACKNOWLEDGMENT

The authors want to thank to FI-UNLP, CONICET, and CICpBA for their support.

REFERENCES

[1] Roberto Cárdenas, Rubén Peña, Patrick Wheeler, Jon Clare, Andrés Muños and Alvaro Sureda, "Control of a wind generation system based on a

Brushless Doubly-fed Induction Generator fed by a matrix converter", Electric Power Systems Reserch, vol 103,(2013), pp 49-60.

[2] A. Singh and Mr. A. Gupta, "Performance Analysis of Wind Energy System Coupled with Brushless Doubly Fed Induction Generator and Matrix Convertor" IJSE Research, vol 5, issue 11 (2014).

[3] F. Rüncos, R Carlson, A.M. Oliveira, P. Kuo-Peng and N. Sadowski, "Performance Analysis of a Brushless Double Fed Cage Induction Generator", Nordic Wind Power Conference (2004), Chalmers University of Technology.

[4] R.A. McMahon, P.C. Roberts, X Wang and P.J Tavner, "Performance of the BDFM as a Generator and Motor", Electric Power Applications, IEE Proceedings, vol: 153, issue: 2 (2006).

[5] M, Boger,.and A., Wallace, "Performance capability analysis of the brushless doubly-fed machine as a wind generator", Electrical Machines and Drives, No: 412, (1995).

[6] H. Voltolini, "Modelagem e controle d geradores de inducao duplamente alimentados com aplicacao em sistemas eólicos", Florianópolis, Brasil`, (2007).

[7] P. Camocardi, "Análisis, Modelado y Control de Sistemas Autónomos que emplean Generadores Eólicos con Máquinas de Doble Bobinado", Ph.D. dissertation, La Plata, Buenos Aires, Argentina, (2011).

[8] Bing Li, Shi LIU, "Study on Direct Torque Control Strategy of Brushless Doubly-fed Induction Generator for Wind Power Generation", Journal of Computational Information Systems, (2014), vol 10, pp 10389-10396.

[9] M. Jovanovic and J. Yu, "Direct Torque and Flux Control of Brushless Doubly-Fed Reluctance Motors", European Conference on Power Electronics and Applications (2003), Toulouse, France.

[10] X. Wang, P.C. Roberts and R.A. McMahon, "Studies of inverter rating of BDFM adjustable speed drive or generator systems", PEDS 2005, IEEE Conference, Pag. 337 - 342.

[11] F. Valenciaga, "Active and Reactive Power Control of a Brushless Doubly Fed Reluctance Machine Using High Order Sliding Modes", International Conference on Electrical Machines, (2008) IEEE.